Supporting Information

Nanocage-Based {In₂Tm₂}-Organic Framework for Efficiently Catalyzing the Cycloaddition Reaction of CO_2 with Epoxides and Knoevenagel Condensation

Hongxiao Lv, Hongtai Chen, Tuoping Hu and Xiutang Zhang*

*Department of Chemistry, College of Science, North University of China, Taiyuan 030051, People's Republic of China . *E-mail: xiutangzhang@163.com*

Contents

Figure S30. ^{1}H NMR spectrum of 2-[(3,4-dimethylphenyl)methylidene]propanedinitrile.

Figure S31. The PXRD patterns of activated and used **NUC-56** after tenth Knoevenagel condensation reactions.

Figure S32. The FT-IR patterns of activated and used **NUC-56** after tenth Knoevenagel condensation reactions.

Figure S33. N$_2$ adsorption isotherms of **NUC-56a** measured after Knoevenagel condensation reaction (purple), showing negligible change in adsorption amount.

Figure S34. Evidence of heterogeneous nature of **NUC-56a** in the Knoevenagel condensation reaction.

Experimental Section

Materials and General Methods. All chemical reagents were commercially purchased from Jinan Heng hua Sci. & Tec. Co. Ltd. without any further refinement. Thermogravimetric analyses (TGA) were performed on NETZSCH STA 449 F3 thermogravimetric analyzer (25-800℃, 10℃/min). The catalytic yield was calculated and measured on a Thermo Fisher Trace ISQ GC/MS instrument. ICP measurements were performed by a (thermofisher) iCAP Qc ICP-MS emission spectrometer. Temperature-programmed desorption (TPD) experiments were performed in VDsorb-91i. Prior to TPD, about 100mg of the catalysts were pretreated for 2 hours in 20 mL/min Ar gas flow at 250 °C. After being cooled to 100 °C, CO_2 or NH_3 absorbed for 2 hours; then, the sample was treated again for 1 hour in 20 mL/min Ar gas flow. Finally, the sample was heated up to 500 °C at a rate of 10 °C/min in the atmosphere of Ar. The desorbed gases were detected by thermal conductivity detector (TCD).

X-ray crystallography. A summary of crystallographic data, refinement parameter and bond lengths and angles for **NUC-56** were given in Table S1 and S2. The diffraction intensity data for **NUC-56** was obtained at 566(2) K by using a Bruker Smart-APEX II CTM area detector (Mo-Kα radiation, λ = 0.071073 nm) with graphite-monochromated radiation. The data integration and reduction were processed with SAINT software. The reflection data were consequently corrected for empirical absorption corrections and Lorentz and polarization effects. The structure was solved by direct methods and refined by full-matrix least-squares with the SHELXL package. All non-hydrogen atoms were refined anisotropically, until convergence was attained. Hydrogen atoms except those on water molecules were generated geometrically with fixed isotropic thermal parameters, and included in the structure factor calculations. The block of SQUEEZE in PLATON was employed to eliminate the highly disordered solvent molecular. Further details on the crystal structure investigations may be obtained from the Cambridge Crystallographic Data Centre, with the depository number CTMC-2168334 for **NUC-56**.

Catalytic Experiment Operation. The catalytic cycloaddition reaction of CO_2 with different epoxy compounds were performed under the optimal reaction conditions in 20 mL around-bottom flask reactor, including 0.5 mol% **NUC-56a** catalyst (0.10 mol %, based on the active In(III) and Tm(III) centers), 1atm CO_2 pressure at 65 ℃ for 7h with a 5.0% mol n-Bu$_4$NBr. CO_2 gas was slowly purged into the reactor until the reaction was over. Eventually, the productivity of cyclocarbonate was estimated by GC-MS analysis through using an internal standard of n-dodecane (18 mmol), and the separated products were analyzed by ^{1}H NMR in DMSO-d_6 solution in all the catalytic reactions. For the Knoevenagel condensation reaction, benzaldehyde (20 mmol), malononitrile (10 mmol), and activated **NUC-56a** (0.4 mol %, based on the In(III) and Tm(III) centers) of 3 mL of ethanol were transferred into a 10 mL closed reaction tube with magnetic stirring for 6 h at 65 ℃. After the reaction, the transformed product was determined by gas chromatography and ^{1}H NMR spectroscopy. The catalytic yield of this Knoevenagel condensation reaction was verified by GC-MS using an internal standard of n-dodecane (15 mmol), and the ^{1}H NMR spectroscopy of products were recorded in Chloroform-d solution.

Table S1. Crystallographic data and refinement parameters of **NUC-56**.

Complex	NUC-56
Formula	$C_{28}H_{12}InNO_{12}Tm$
Mr	838.14
Crystal system	monoclinic
Space group	C2/m
a (Å)	15.180(3)
b (Å)	16.448(2)
c (Å)	18.920(8)
α (°)	90
β (°)	101.03
γ (°)	90
V(Å^3)	4637(2)
Z	4
DcalTm(g·cm^{-3})	1.201
μ(mm^{-1})	7.819
GOF	1.072
R_1 [I$>$2σ(I)]a	0.0722
wR$_2$ [I$>$2σ(I)]b	0.2020
R_1a (all data)	0.0741
wR$_2$b (all data)	0.2039
Rint	0.0641

$^aR_1=\sum\left|\left|F_o\right|-\left|F_c\right|\right|/\sum\left|Fo\right|$. $^bwR_2=\left|\sum w(\left|F_o\right|^2-\left|F_c\right|^2)\right|/\sum\left|w(F_o^2)^2\right|^{1/2}$

Table S2. Selected bond lengths and angles of **NUC-56**.

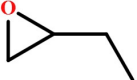| Selected bond lengths (Å)			
Tm(1) -O(2) #1	2.187(8)	Tm(1)-O(2)	2.187(8)
Tm(1)-O(1W)#2	2.307(9)	Tm(1)-O(4)#3	2.204(6)
Tm(1)-O(4)#4	2.204(6)	Tm(1)-O(5)#5	2.360(10)
Tm(1)-O(5)#6	2.360(10)	In(1)-O(1)	2.166(8)
In(1)-O(1)#1	2.166(8)	In(1)-O(1W)	2.127(9)
In(1)-O(2W)	2.181(16)	In(1)-O(3)#7	2.167(7)
In(1)-O(3)#8	2.167(7)		
Selected angles (°)			
O(2) #1-Tm(1)-O(2)	89.8(6)	O(2) #1-Tm(1)-O(1W)#2	82.1 (3)
O(2) -Tm(1)-O(1W)#2	82.1(3)	O(2) #1-Tm(1)-O(4)#3	165.4(4)
O(2) -Tm(1)-O(4)#4	165.4(4)	O(2) -Tm(1)-O(4#3)	93.3(4)
O(2)#1-Tm(1)-O(4)#4	93.3(4)	O(2) -Tm(1)-O(5)#6	83.8(4)
O(2) -Tm(1)-O(5)#5	117.9(4)	O(2)#1-Tm(1)-O(5)#6	117.9 (4)
O(2)#1-Tm(1)-O(5)#5	83.8(4)	O(1W)#2-Tm(1)-O(5)#5	155.4(3)
O(1W)#2-Tm(1)-O(5)#6	155.4(3)	O(4)#4-Tm(1)-O(1W)#2	84.1(3)
O(4)#3-Tm(1)-O(1W)#2	84.1(3)	O(4)#4-Tm(1)-O(4)#3	80.4(4)
O(4)#4-Tm(1)-O(5)#6	107.2(4)	O(4)#3-Tm(1)-O(5)#5	107.2(4)
O(4)#4-Tm(1)-O(5)#5	76.7(4)	O(4)#3-Tm(1)-O(5)#6	76.7(4)
O(5)#6-Tm(1)-O(5)#5	48.2(5)	O(1)-In(1)-O(1)#1	108.1(5)
O(1)#1- In(1)-O(2W)	86.3(5)	O(1)- In(1)-O(2W)	86.3(5)
O(1)- In(1)-O(3)#7	84.1(3)	O(1)#1- In(1)-O(3)#8	84.1(3)
O(1) - In(1)-O(3)#8	165.6(3)	O(1)#1- In(1)-O(3)#7	165.6(3)
O(1W)- In(1)-O(1)#1	95.2(3)	O(1W)-In(1)-O(1)	95.2(3)
O(1W)- In(1)-O(2W)	177.4(8)	O(1W) - In(1)-O(3)#8	91.2(3)
O(1W)- In(1)-O(3)#7	91.2(3)	O(3)#8- In(1)-O(2W)	86.9(6)
O(3)#7- In(1)-O(2W)	86.9(6)	O(3)#8- In(1)-O(83)#7	82.9(5)

Symmetry transformations used to generate equivalent atoms: [1]x,-y,z; [2]-x+1,-y,-z;[3]x-1/2,-y+1/2,z; [4]x-1/2,y-1/2,z; [5]-x+3/2,-y+1/2,-z+1; [6]-x+3/2,y-1/2,-z; [7]-x+3/2,-y+1/2,-z; [8]-x+3/2,y-1/2,-z; [9]x,-y+1,z; [10]x+1/2,y+1/2,z;

Table S3. Comparison of the catalytic activity of various MOFs for the cycloaddition of CO_2 with epoxides.

MOF	Catalyst (mol%)	TBAB (mol%)	Temperature (°C)	Pressure (atm)	Time (h)	Yield (%)	TON	TOF (h^{-1})	Ref.
2	0.5	1.0	40	1	20	99	200	10	S1
1a	0.4	0.5	60	1	12	97	242.5	20.2	S2
UiO-66-Gua0.2(s)	0.6	0.8	70	1	12	96	160	13	S3
Zn-2PDC	0.5	3.6	rt	10	12	98	200.4	16.7	S4
PNU-25-NH$_2$	1.0	0.5	55	1	18	93	93.6	5.2	S5
Zn$_{0.75}$Mg$_{0.25}$-MOF-74	0.59	0.9	60	8	5	99	168	34	S6
Hie-Zn-MOF-TEA	0.5	2.2	rt	10	16	90	185.6	11.6	S7
Zn$_3$(L)$_3$(H$_2$L)	0.26	0.9	80	10	5	99	367.5	73.5	S8
JLU-Liu21	1.8	5.0	60	20	6	99	66	11	S9
NUC-56a	0.1	5.0	65	1	7	99	990	141	This work

Table S4. Molecular sizes of epoxides with different substituted groups.

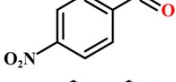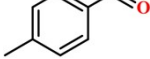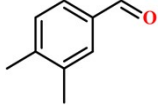| Entry	Epoxides	Molecular Size (Å³)
1		4.850*6.356*5.053
2		5.823*4.650*5.207
3		4.773*4.970*6.472
4		5.701*7.312*5.335
5		7.311*5.170*5.472
6		7.635*5.043*5.386
7		7.740*5.631*5.073
8		9.421*7.192*4.910
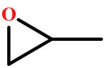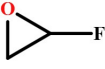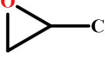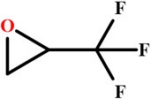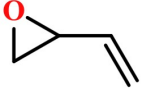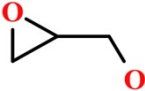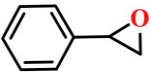
Table S5. ICP-OES analysis of In^{3+} and Tm^{3+} after 10 cycles reaction of cycloaddition reaction.

Catalyst	In^{3+} concentration (%)	Tm^{3+} concentration (%)
NUC-56a	0.020	0.024

**Table S6**. Comparison of the catalytic activity of various MOFs for the Knoevenagel Condensation reaction.

MOF	Catalyst (mol%)	Solvent	Temperature (°C)	Time (h)	Yield (%)	TON	TOF (h^{-1})	Ref.
1	1	-	27	3	100	100	33	S10
UiO-66-NH$_2$	9	EtOH	80	2	94	2	1	S11
[Zn(κN-H$_3$L)(H$_2$O)$_3$]·3H$_2$O	3	THF	50	4	94	31	8	S12
NUC-25	0.4	Ethanol	80	24	99	248	10	S13
Zn$_2$dobdc	50mg	Toluene	70	24	14	-	-	S14
[Co$_2$(bptc)(H$_2$O)$_2$] ·5DMA	2	-	60	6	99	50	8	S15
NUC-56a	0.4	Ethanol	65	6	99	248	41	This work

Table S7. Molecular sizes of various benzaldehyde derivatives.

Entry	Substrates	Molecular Size (Å^3)
1		8.604*7.159*2.383
2		9.211*7.006*2.904
3		10.022*6.853*2.520
4		9.910*7.056*4.230
5		9.526*7.210*4.186
6		11.925*8.350*7.212
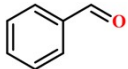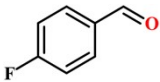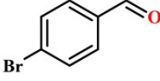
Table S8. ICP-OES analysis of In^{3+} and Tm^{3+} after 10 cycles reaction of Knoevenagel condensation reaction.
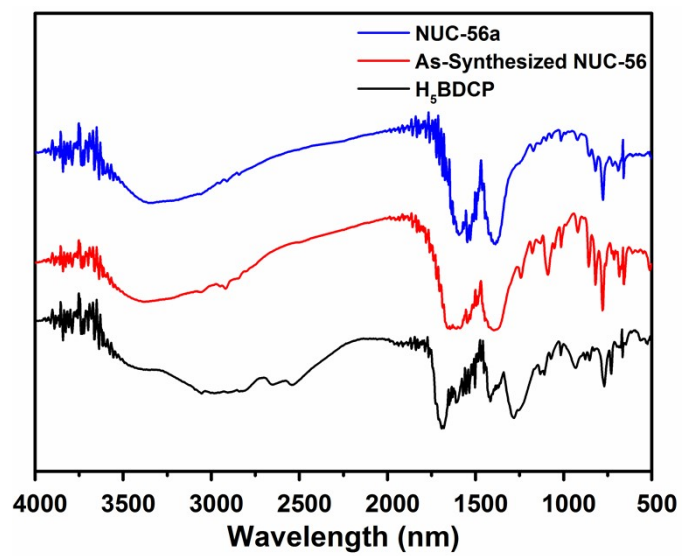
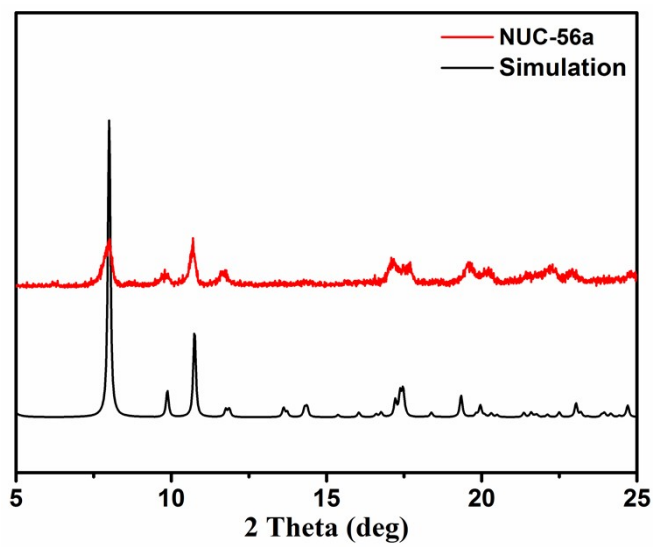| Catalyst	In^{3+} concentration (%)	Tm^{3+} concentration (%)
NUC-56a	0.025	0.031
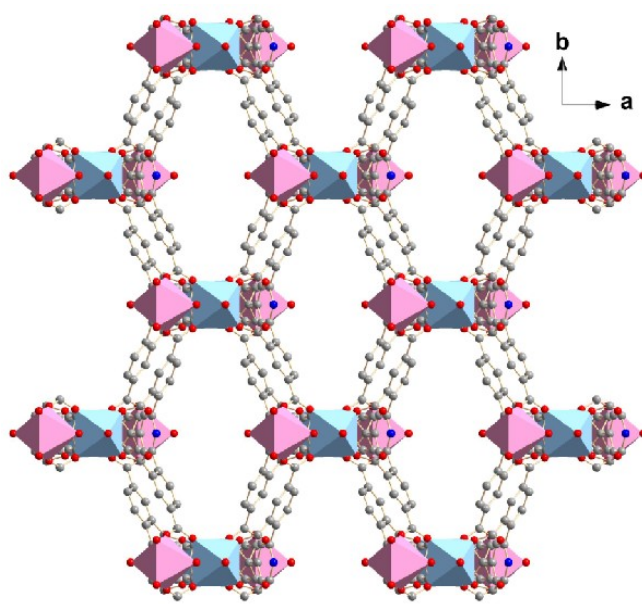
Figure S1. The 3D framework of **NUC-56** view along c axis.
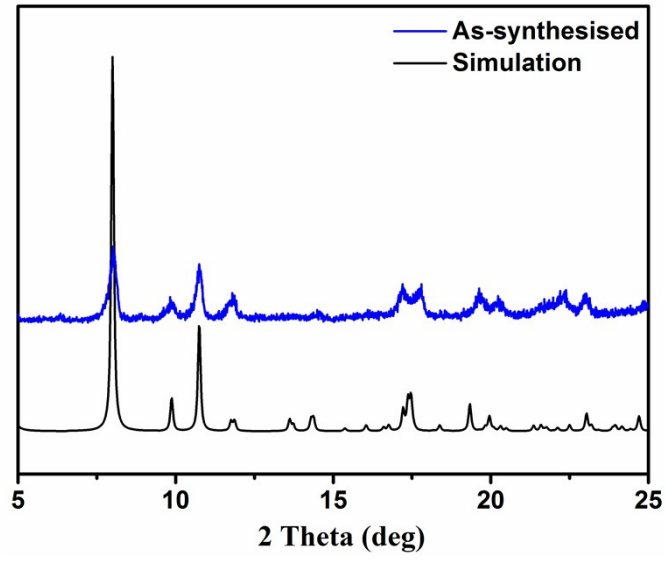
Figure S2. The PXRD patterns of as-synthesized **NUC-56** and simulated one.

Figure S3. The FT-IR spectrum of ligand, as-synthesized **NUC-56**, and activated **NUC-56a**.
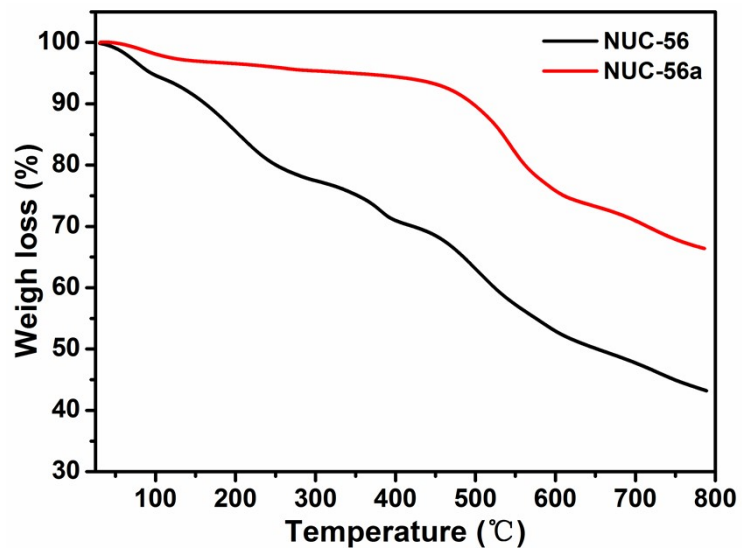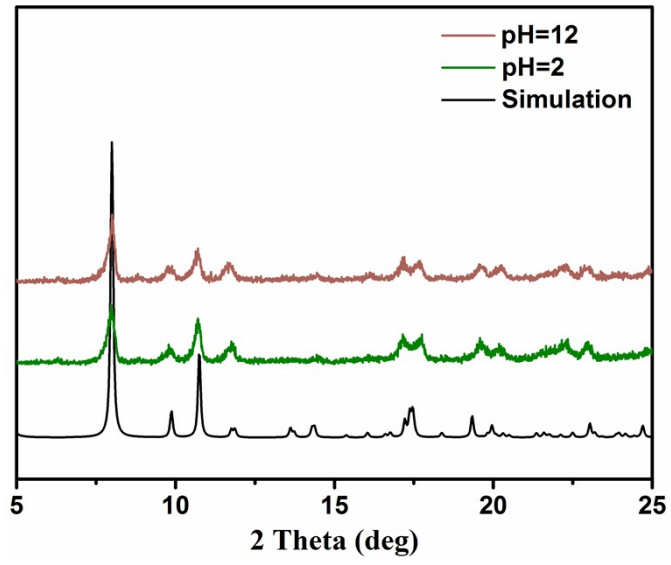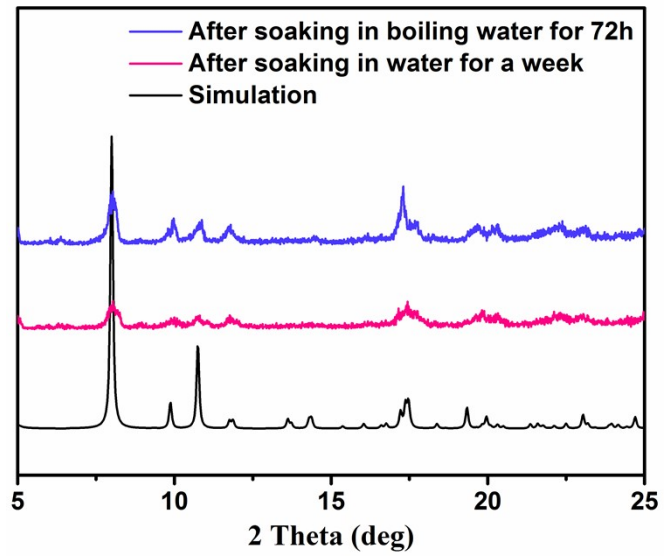
Figure S4. The PXRD patterns of simulated **NUC-56** and **NUC-56a**.

Figure S5. The TGA curves of **NUC-56** and **NUC-56a**.

Figure S6. The PXRD patterns of **NUC-56** sample under varied pH solutions.

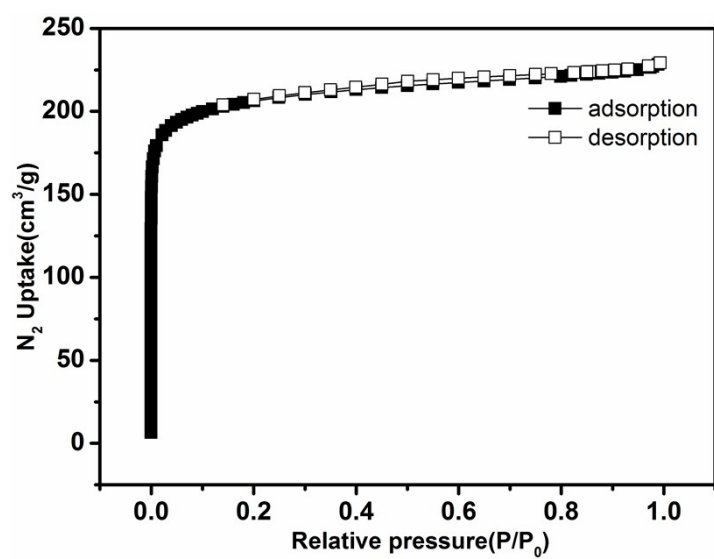**Figure S7.** The PXRD patterns of **NUC-56** sample under water treatment.

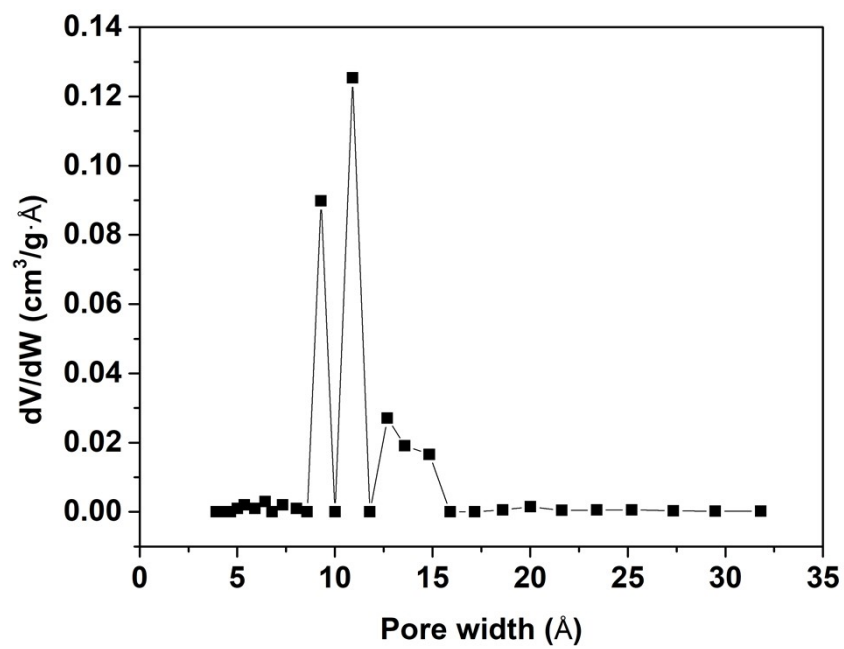**Figure S8.** N_2 absorption and desorption isotherms of **NUC-56a** at 77 K.

Figure S9. The pore distribution of **NUC-56a**.

Isosteric Heat Calculation.

The Q_{st} value is a parameter that describes the average enthalpy of adsorption for an adsorbing gas molecule at a specific surface coverage and is usually evaluated using two or more adsorption isotherms collected at similar temperatures. The zero-coverage isosteric heat of adsorption is evaluated by first fitting the temperature-dependent isotherm data to a virial-type expression, which can be written as:

$$\ln p = \ln N + \frac{1}{T}\sum_{i=0}^{m} a_i\, N^i + \sum_{j=0}^{n} b_j\, N^j$$

N: Adsorption capacity (mg/g); **p:** Pressure (mmHg); **T:** Temperature (K); $\mathbf{a_i}$、$\mathbf{b_j}$：Empirical constant; **R**：Universal gas constant (8.314 J·mol^{-1}·K^{-1})

The isosteric enthalpy of adsorption (Qst)：

$$Q_{st} = -R\sum_{i=0}^{m} a_i\, N^i$$
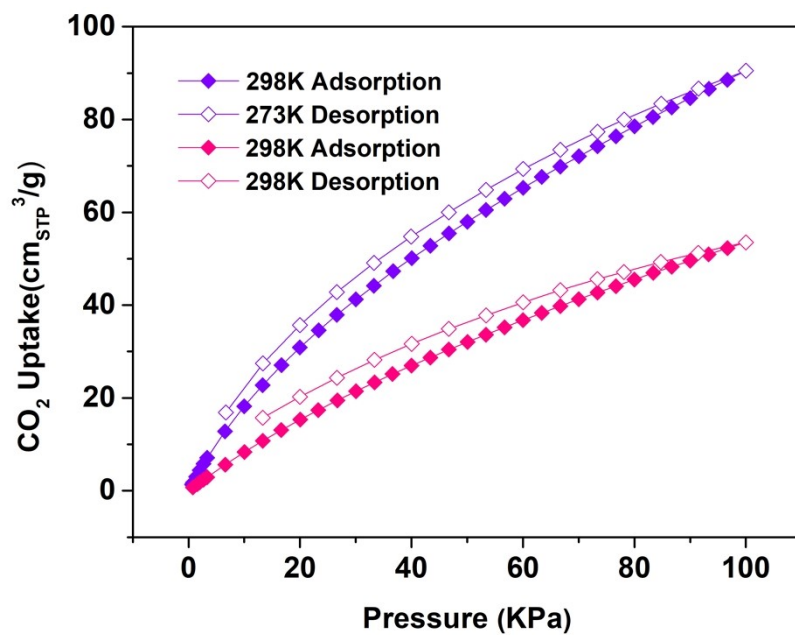
Figure S10. The CO_2 adsorption and desorption isotherms for **NUC-56a** at 273K and 298K. Filled symbols: adsorption; Open symbols: desorption.
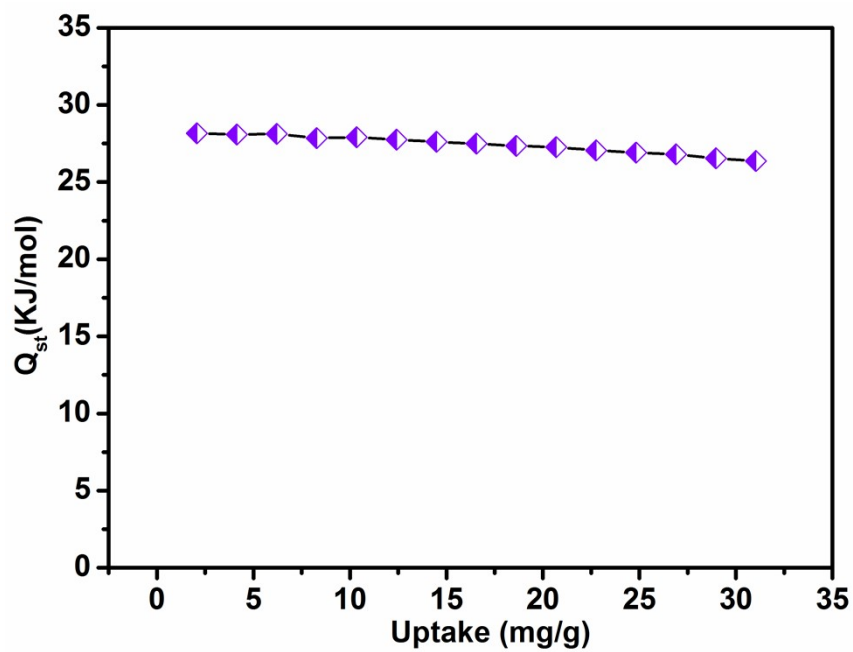
Figure S11. CO_2 adsorption heat calculated by the virial equation of **NUC-56a**.

Yield Calculation Based on the GC-MS Analysis

Gas chromatography mass spectrometry (GC-MS) analyses were executed on a time-of-flight Thermo Fisher Trace ISQ GC/MS instrument, the yield (%) was calculated based on the consumption of starting material using the equation:

$$\text{Yield (\%)} = \left(\frac{\frac{\text{area of reactant at 0 hour}}{\text{area of interal atandard at 0 hour}} - \frac{\text{area of reactant at any time}}{\text{area of interal atandard at any time}}}{\frac{\text{area of reactant at 0 hour}}{\text{area of interal standard at 0 hour}}} \right)$$
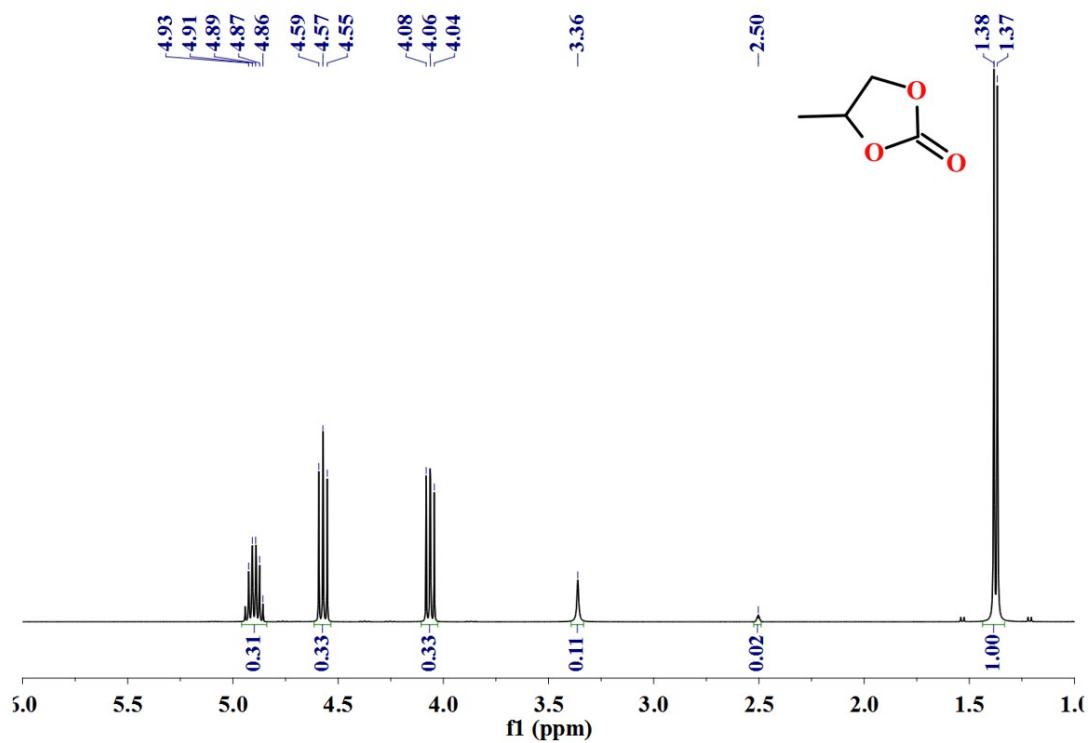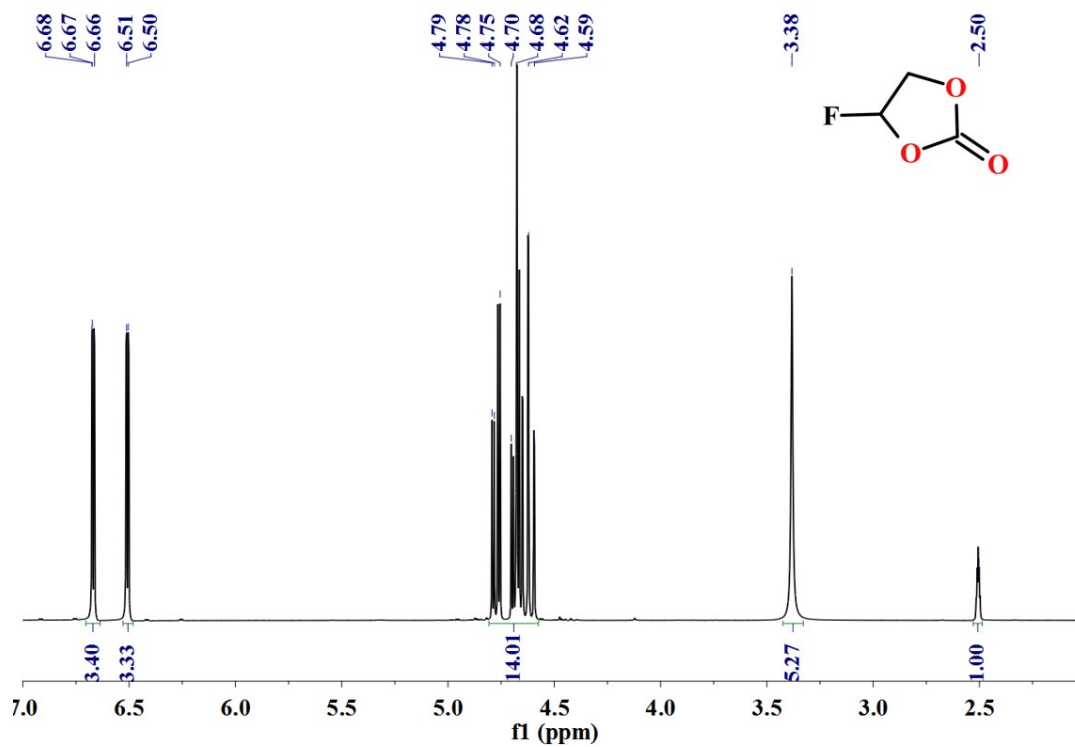
Figure S12. ^{1}H NMR spectrum of Propylene carbonate.

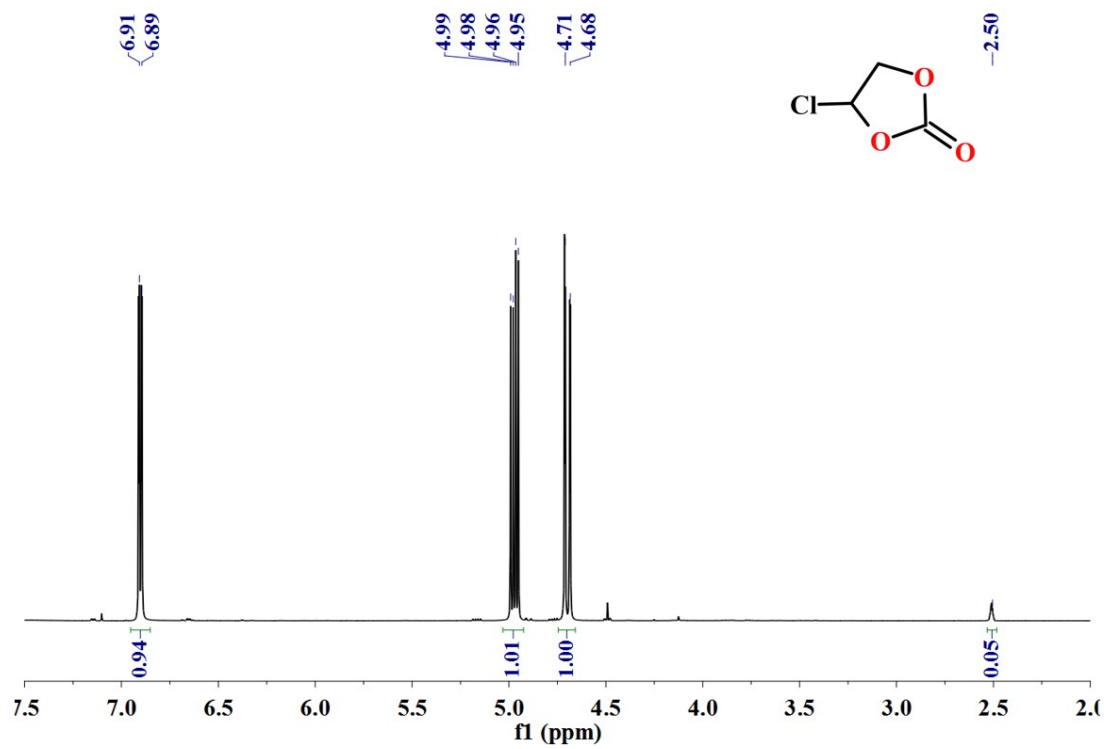**Figure S13.** ^{1}H NMR spectrum of Fluoride vinyl carbonate.

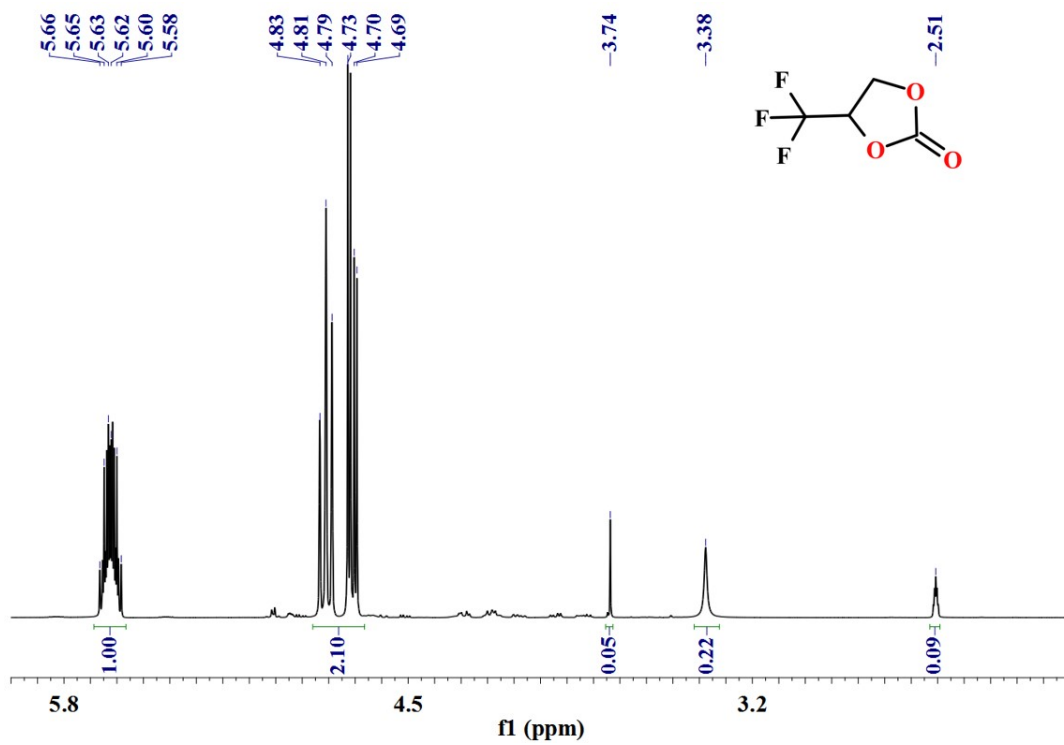**Figure S14.** ^{1}H NMR spectrum of 4-chlorine-1,3-pentamine-2-ketone.

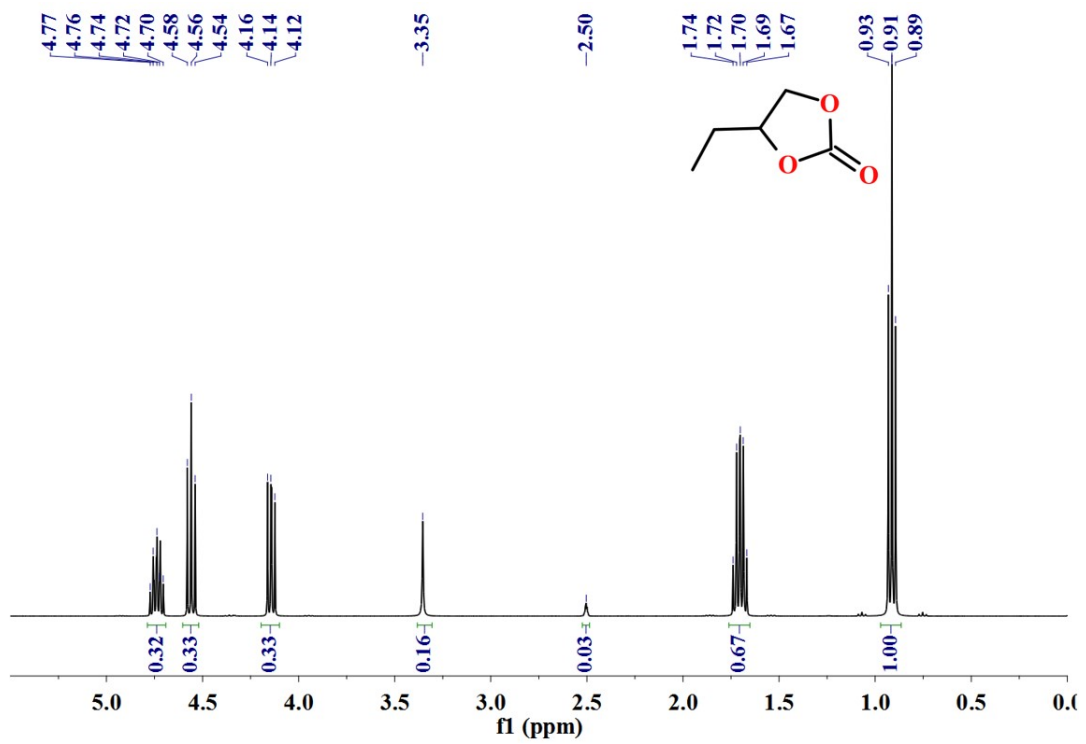**Figure S15.** ¹H NMR spectrum of 2-(trifluoromethyl)oxirane.

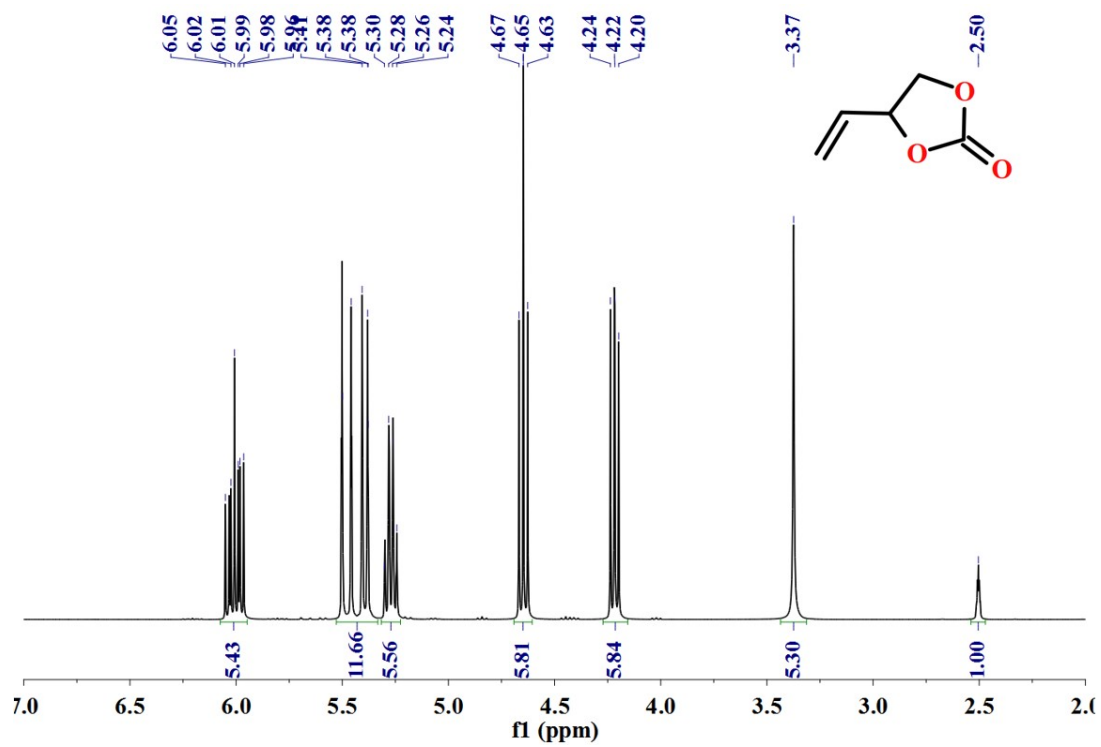**Figure S16.** ^{1}H NMR spectrum of 1,2-butylene carbonate.
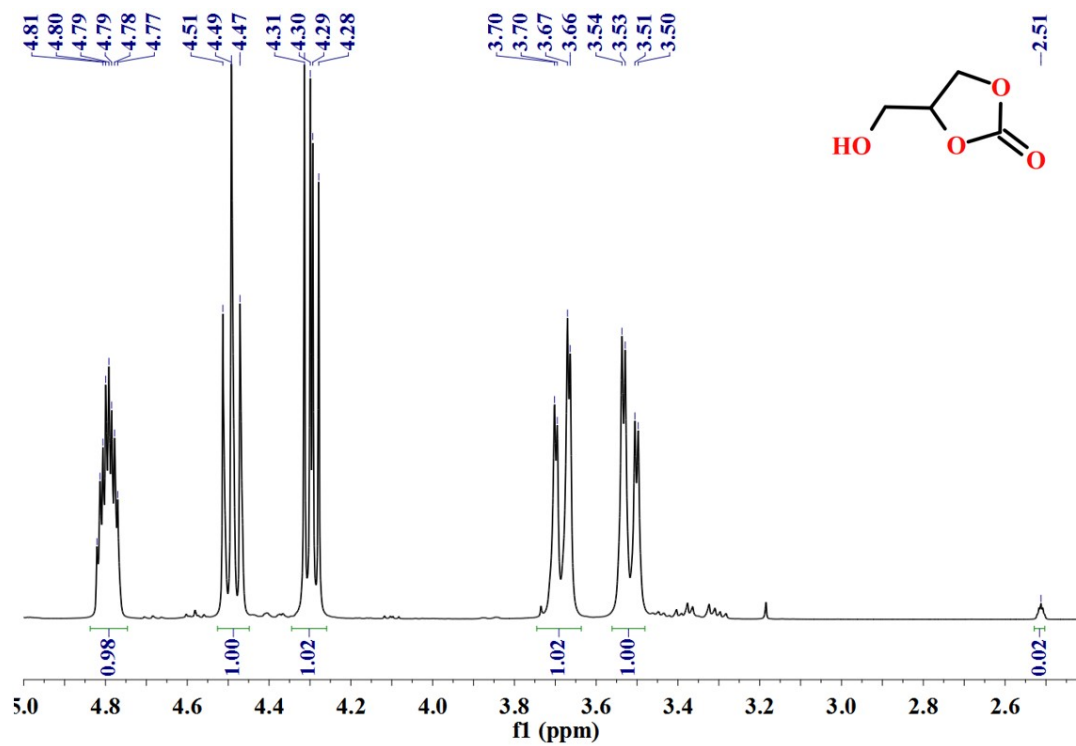
Figure S17. ^{1}H NMR spectrum of Ethyl vinyl carbonate.

Figure S18. ¹H NMR spectrum of 4-(hydroxymethyl)-1,3-dioxolan-2-one.

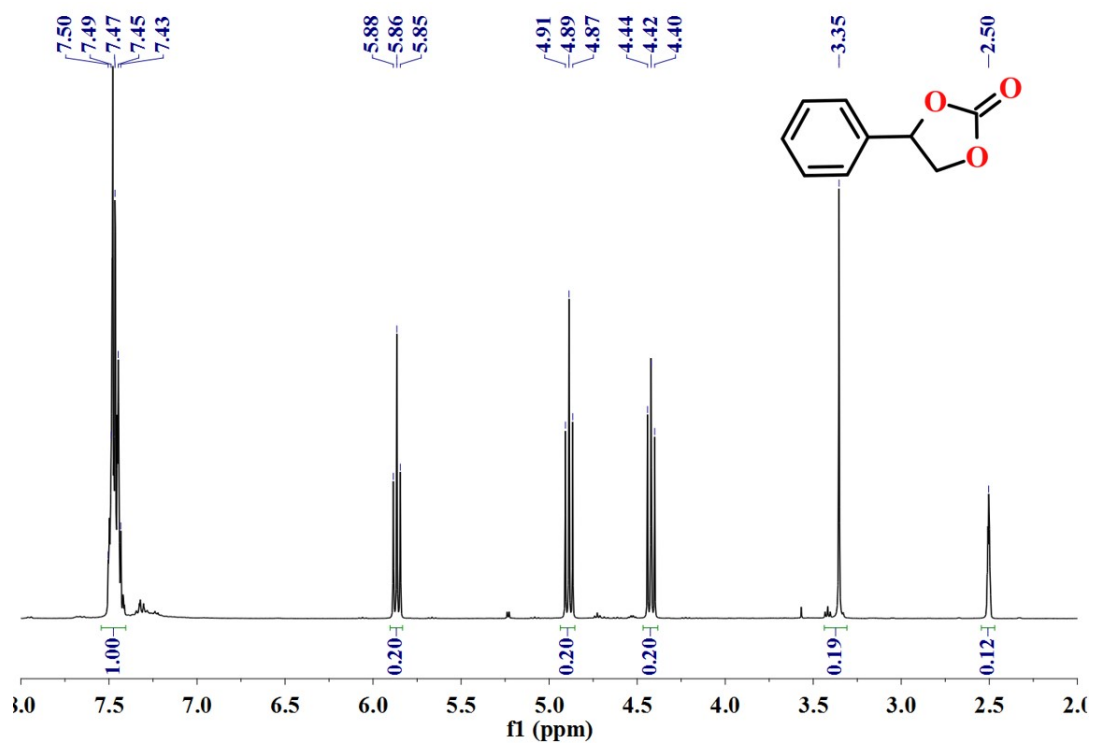**Figure S19.** ^{1}H NMR spectrum of 4-phenyl-1,3-dioxolan-2-one.
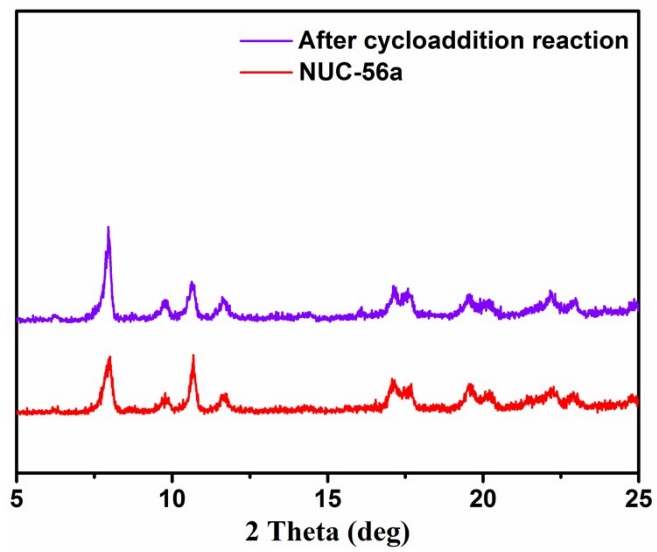
Figure S20. The PXRD patterns of activated and used **NUC-56** after tenth cycloaddition reactions.
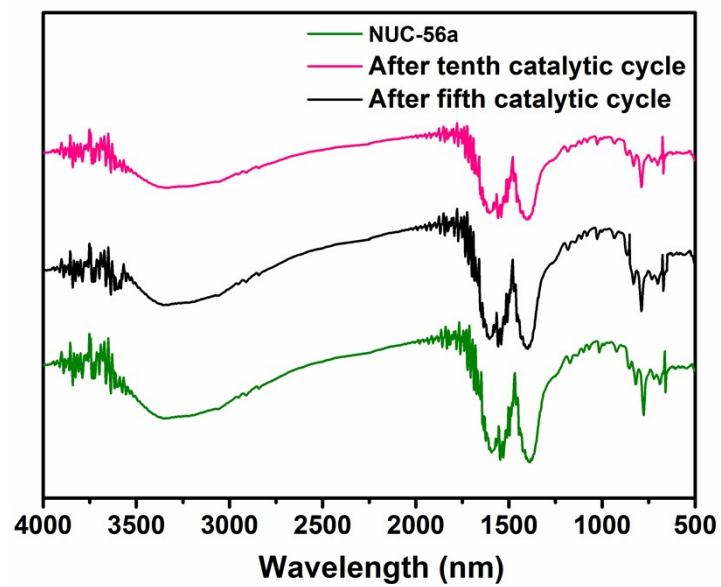
Figure S21. The FT-IR patterns of activated and used **NUC-56** after fifth and tenth cycloaddition reactions.
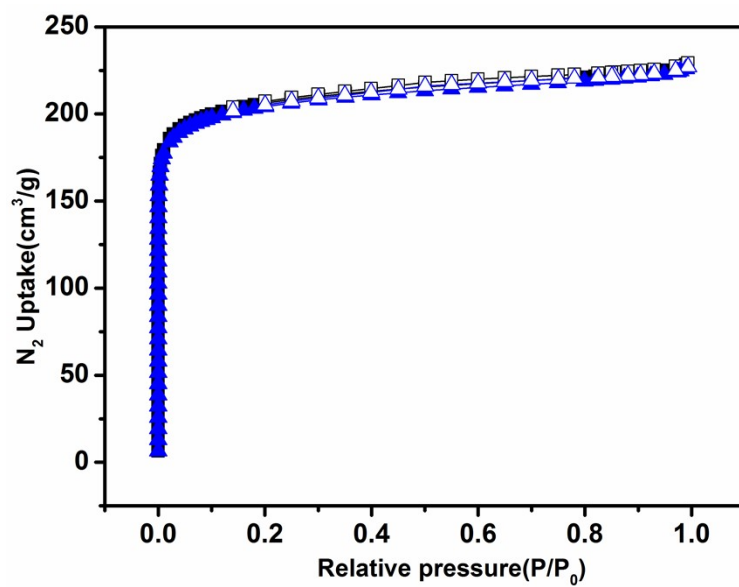
Figure S22. N_2 adsorption isotherms of **NUC-56a** measured after 10 cycles of cycloaddition reactions (blue), showing negligible change in adsorption amount.
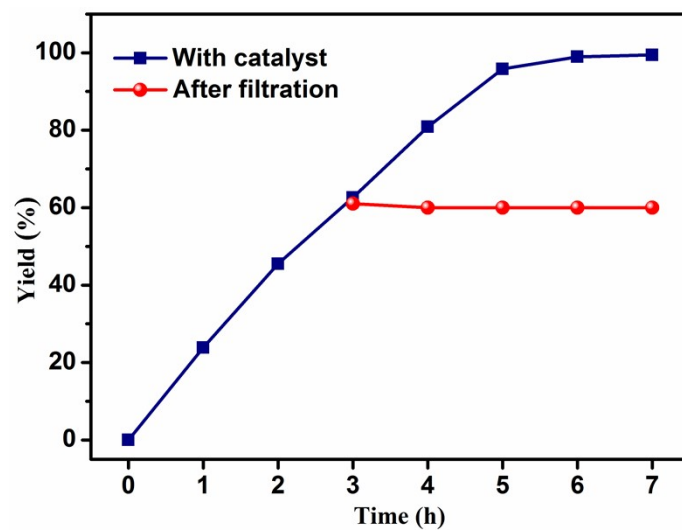
Figure S23. Evidence of heterogeneous nature of **NUC-56a** in the cycloaddition reaction.
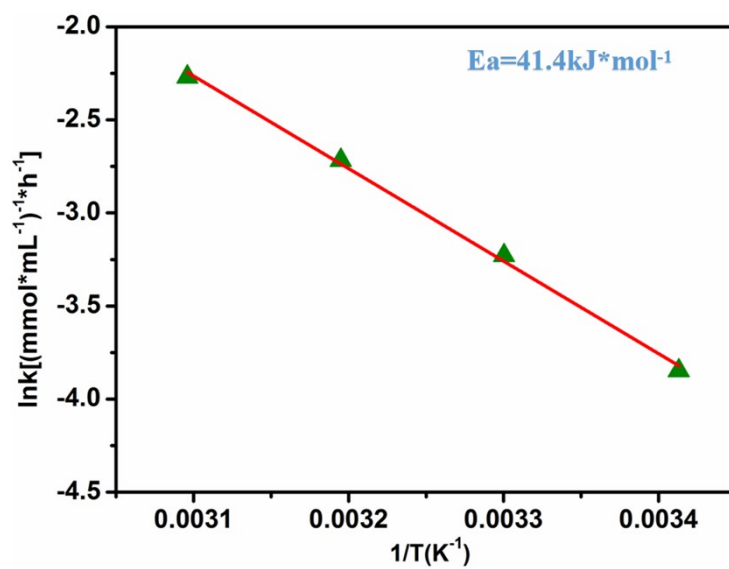
Figure S24. The activating energy of Knoevenagel condensation reaction.
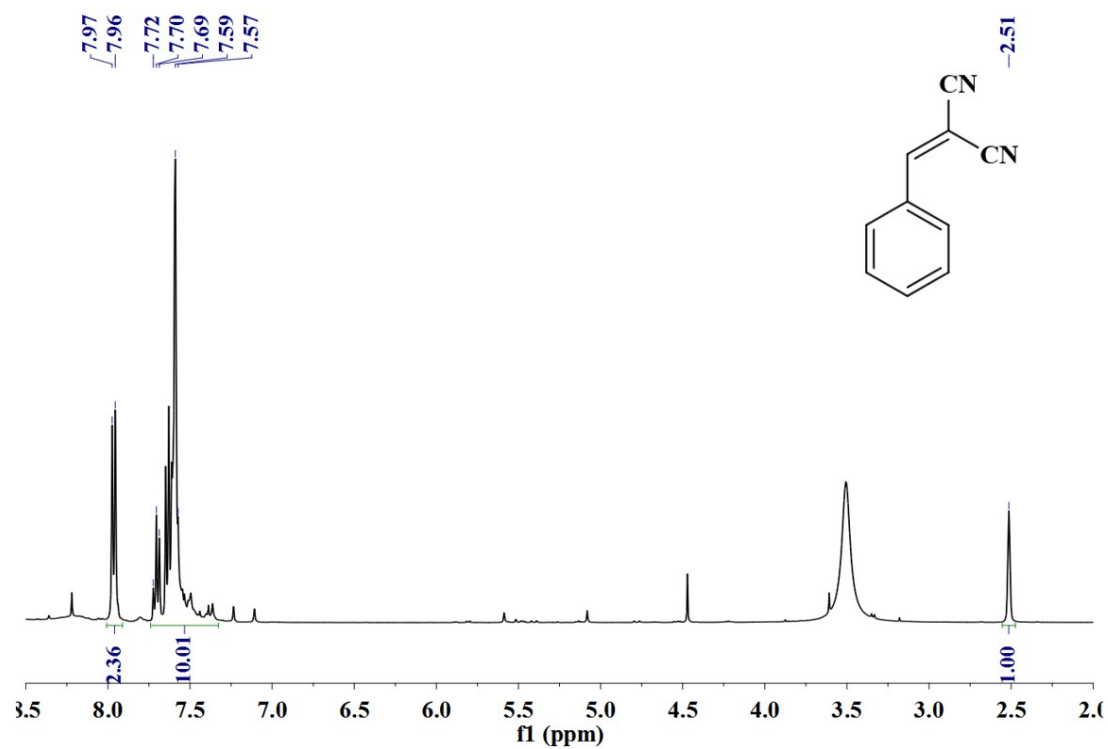
Figure S25. ^{1}H NMR spectrum of 2-(phenylmethylidene)propanedinitrile.
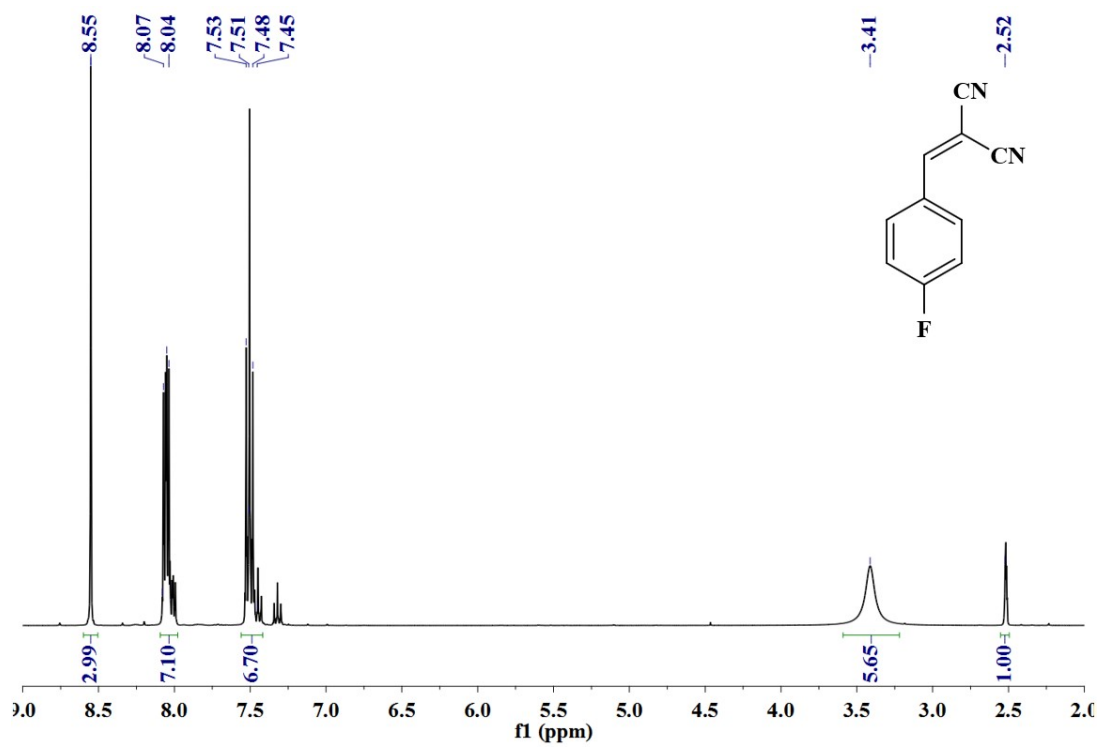
Figure S26. ^{1}H NMR spectrum of 2-[(4-fluorophenyl)methylidene] propanedinitrile.
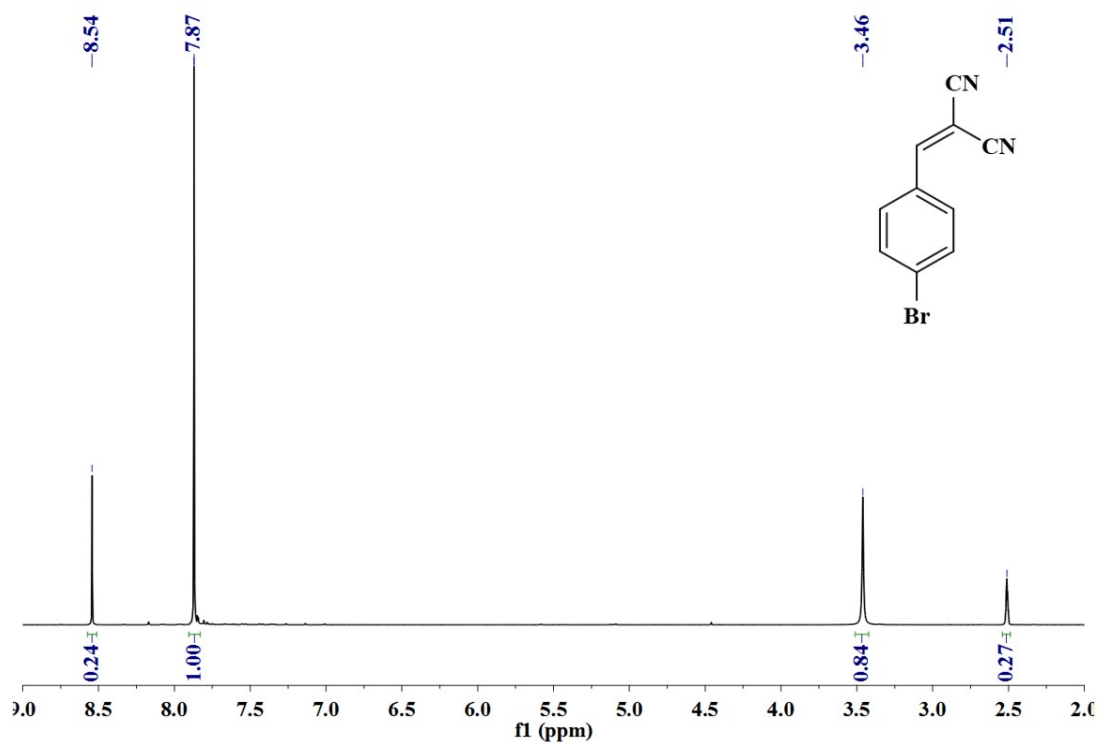
Figure S27. ^1H NMR spectrum of 2-[(4-bromophenyl)methylidene] propanedinitrile.
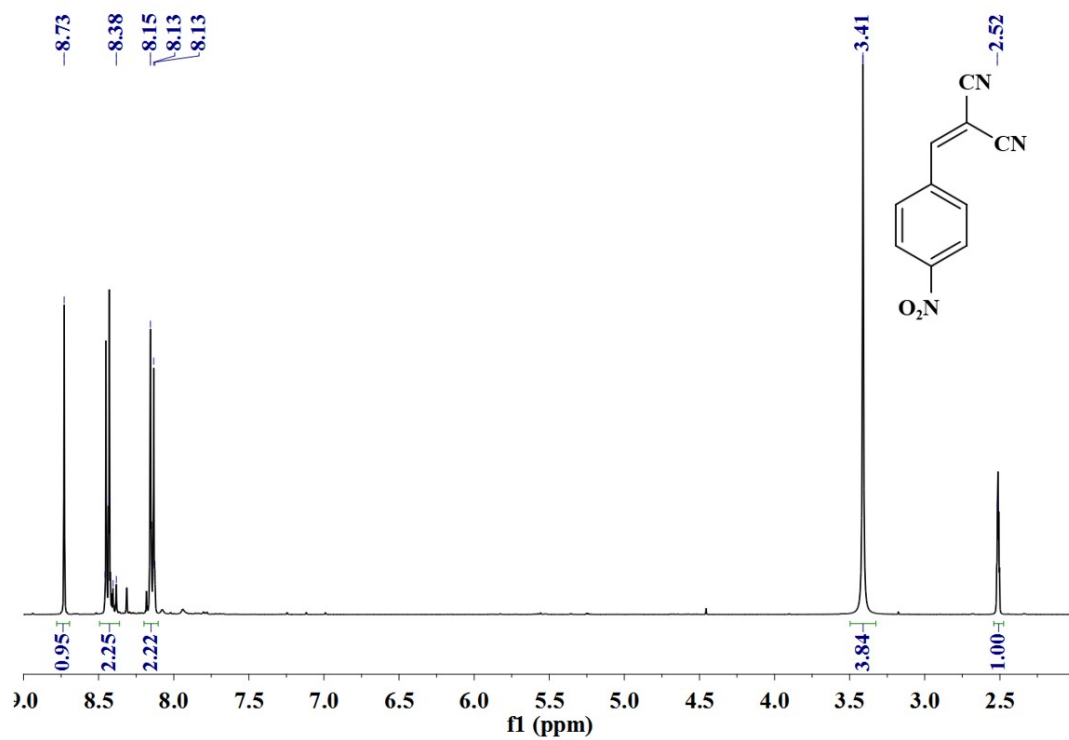
Figure S28. ^{1}H NMR spectrum of 2-[(4-nitrophenyl) methylidene] propanedinitrile.
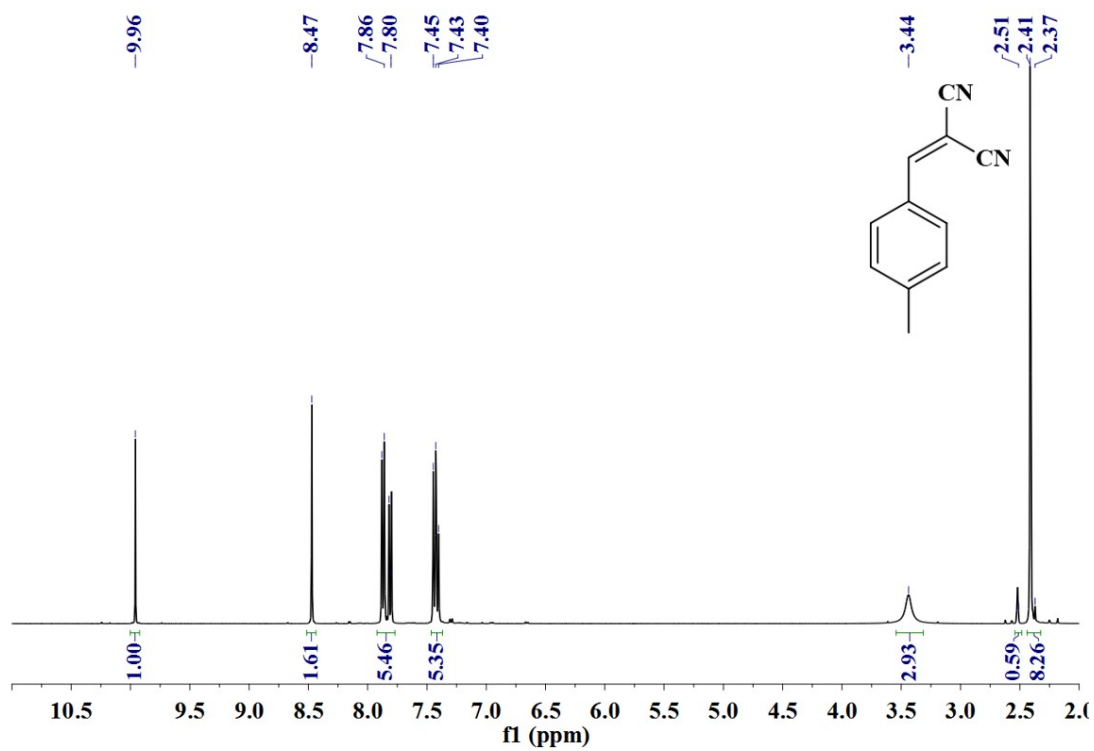
Figure S29. ¹H NMR spectrum of 2-[(4-methylphenyl)methylidene]propanedinitrile.
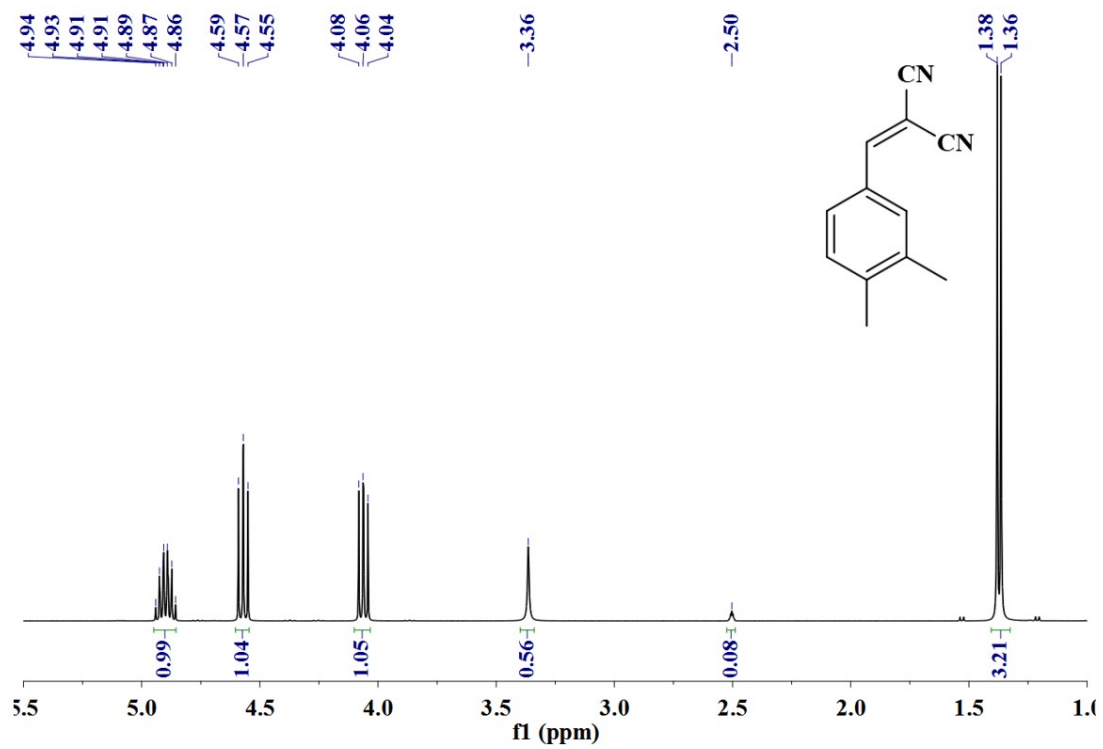
Figure S30. ^{1}H NMR spectrum of 2-[(3,4-dimethylphenyl)methylidene]propanedinitrile.
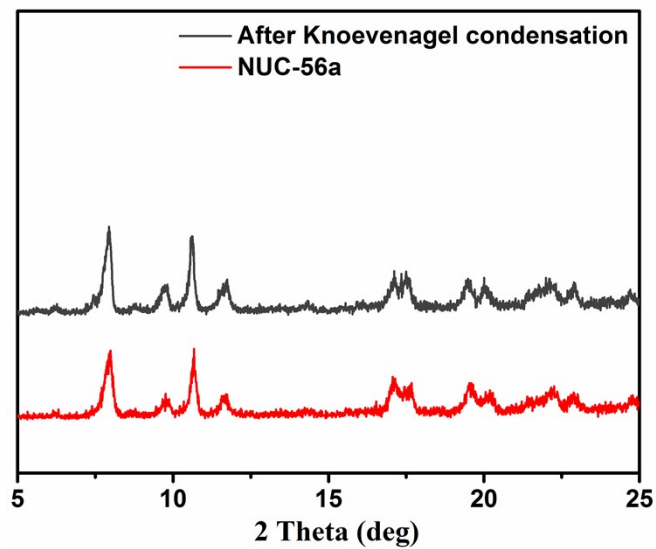
Figure S31. The PXRD patterns of activated and used **NUC-56** after tenth Knoevenagel condensation reactions.
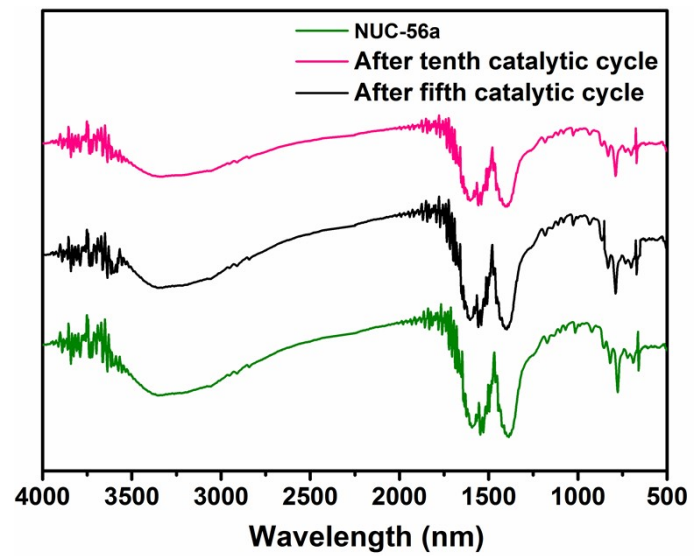
Figure S32. The FT-IR patterns of activated and used **NUC-56** after fifth and tenth Knoevenagel condensation reactions.
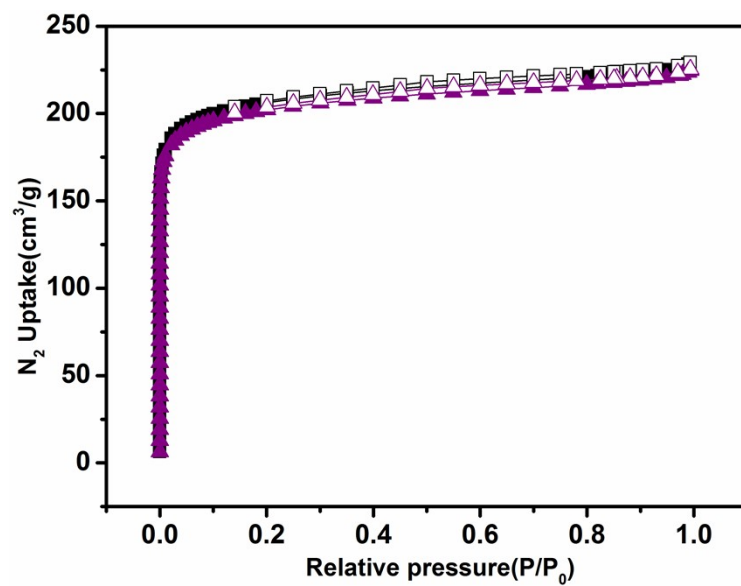
Figure S33. N_2 adsorption isotherms of **NUC-56a** measured after Knoevenagel condensation reaction (purple), showing negligible change in adsorption amount.
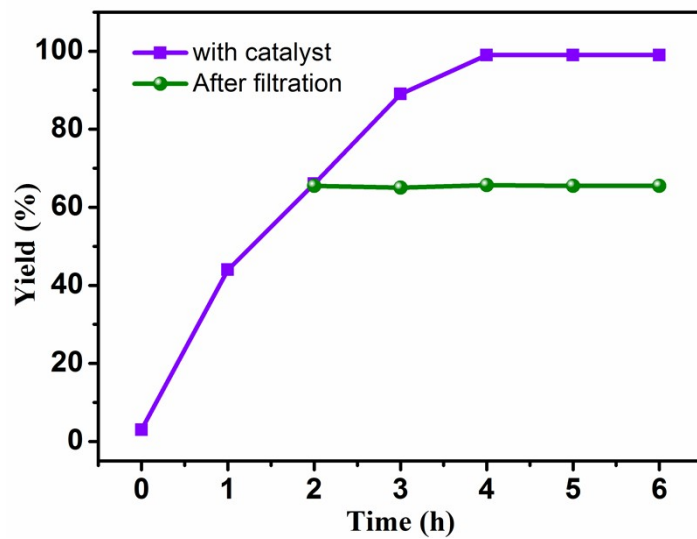
Figure S34. Evidence of heterogeneous nature of **NUC-56a** in the Knoevenagel condensation reaction.

Reference

S1. Gupta, V.; Mandal, S. K., Effect of Unsaturated Metal Site Modulation in Highly Stable Microporous Materials on CO_2 Capture and Fixation. *Inorg. Chem*., **2022**, *61*, 3086-3096.

S2. Wang, W. M.; Wang, W. T.; Wang, M. Y.; Gu, A. L.; Wu, Z. L., A Porous Copper–organic Framework Assembled by [Cu_{12}] Nanocages: Highly Efficient CO_2 Capture and Chemical Fixation and Theoretical DFT Calculations. *Inorg. Chem*., **2021**, *60*, 9121-9133.

S3. Gao, A.; Li, F.; Xu, Z.; Ji, C.; Gu, J.; Zhou, Y. H., Guanidyl-implanted UIO-66 as an Efficient Catalyst for the Enhanced Conversion of Carbon Dioxide into Cyclic Carbonates. *Dalton Trans.*, **2022**, 51, 2567-2576.

S4. Li, Y.; Zhang, X.; Lan, J.; Li, D.; Wang, Z.; Xu, P.; Sun, J. A High-performance Zinc-organic Framework with Accessible Open Metal Sites Catalyzes CO_2 and Styrene Oxide into Styrene Carbonate under Mild Conditions. *ACS Sustainable Chem. Eng.*, **2021**, 9, 2795−2803.

S5. Kurisingal, J. F.; Rachuri, Y.; Gu, Y.; Chitumalla, R. K.; Vuppala, S.; Jang, J.; Bisht, K. K.; Suresh, E.; Park, D. W. Facile Green Synthesis of New Copper-based Metal-organic Frameworks: Experimental and Theoretical Study of the CO_2 Fixation Reaction. *ACS Sustainable Chem. Eng.*, **2020**, 8, 10822−10832.

S6. Gao, Z.; Liang, L.; Zhang, X.; Xu, P.; Sun, J., Facile one-pot synthesis of Zn/Mg-MOF-74 with Unsaturated Coordination Metal Centers for Efficient CO2 Adsorption and Conversion to Cyclic Carbonates. *ACS Appl. Mater. Interfaces*, **2021**, 13, 61334−61345.

S7. Lan, J.; Qu, Y.; Wang, Z.; Xu, P.; Sun, J. A Facile Fabrication of a Multi-functional and Hierarchical Zn-based MOF as an Efficient Catalyst for CO_2 Fixation at Room-temperature. *Inorg. Chem. Front.*, **2021**, 8, 3085−3095.

S8. Gao, Z.; Zhang, X.; Xu, P.; Sun, J. Dual Hydrogen-bond Donor Group-containing Zn-MOF for the Highly Effective Coupling of CO_2 and Epoxides under Mild and Solvent-free Conditions. *Inorg. Chem. Front.*, **2020**, 7, 1995−2005.

S9. Gu, J.; Sun, X.; Liu, X.; Yuan, Y.; Shan, H.; Liu, Y. Highly Efficient Synergistic CO_2 Conversion with Epoxide Using Copper Polyhedron-based MOFs with Lewis Acid and Base Sites. *Inorg. Chem. Front.*, **2020**, 7, 4517−4526.

S10. Datta, M.; Sadhika, K.; Mandal, S. K. Engineering a Nanoscale Primary Amide-functionalized 2D Coordination Polymer as an Efficient and Recyclable Heterogeneous Catalyst for the Knoevenagel Condensation Reaction. *Acs Appl. Nano Mater.*, **2018**, 1, 5226-5236.

S11. Yang, Y.; Yao, H.-F.; Xi, F.-G.; Gao, E.-Q. Amino-functionalized Zr(IV) Metal−organic Framework as Bifunctional Acid−base Catalyst for Knoevenagel Condensation. *J. Mol. Catal. A: Chem.*, **2014**, 390, 198−205.

S12. Karmakar, A.; Paul, A.; Mahmudov, K. T.; Guedes da Silva, M. F. C.; Pombeiro, A. J. L. pH Dependent Synthesis of Zn(II) and Cd(II) Coordination Polymers with Dicarboxyl-Functionalized Arylhydrazone of Barbituric Acid: Photoluminescence Properties and Catalysts for Knoevenagel Condensation. *New J. Chem.*, **2016**, 40, 1535-1546.

S13. Chen, H.; Hu, T.; Fan, L.; Zhang, X. One Robust Microporous Tm(III)-Organic Framework for Highly Catalytic Activity on Chemical CO_2 Fixation and Knoevenagel Condensation. *Inorg. Chem.*, **2021**, 60, 1028-1036.

S14. Valvekens, P.; Vandichel, M.; Waroquier, M.; Van Speybroeck, V.; De Vos, D. Metal-dioxidoterephthalate MOFs of the MOF-74 type: Microporous basic catalysts with well-defined active sites. *J. Catal.*, **2014**, 317, 1−10.

S15. Deng, J.-B.; Wang, X.; Ni, Z.-Q.; Zhu, F. Two Co(II)-Based MetalOrganic Frameworks: Catalytic Knoevenagel Condensation Reactions and Inhibitory Activity on the Scar Tissue Hyperplasia by Reducing the Activity of the VEGF Signaling Pathway. *Arab. J. Chem.*, **2020**, 13, 7482-7489.